Indirect measurement of three-photon correlation in nonclassical light sources

Byoung-moo Ann, Younghoon Song, Junki Kim, Daeho Yang, and Kyungwon An*
Department of Physics and Astronomy, Seoul National University, Seoul 151-747, Korea
(Received 27 March 2016; published 9 June 2016)

We observe the three-photon correlation in nonclassical light sources by using an indirect measurement scheme based on the dead-time effect of photon-counting detectors. We first develop a general theory which enables us to extract the three-photon correlation from the two-photon correlation of an arbitrary light source measured with detectors with finite dead times. We then confirm the validity of our measurement scheme in experiments done with a cavity-QED microlaser operating with a large intracavity mean photon number exhibiting both sub- and super-Poissonian photon statistics. The experimental results are in good agreement with the theoretical expectation. Our measurement scheme provides an alternative approach for N-photon correlation measurement employing $(N-1)$ detectors and thus a reduced measurement time for a given signal-to-noise ratio, compared to the usual scheme requiring N detectors.

DOI: 10.1103/PhysRevA.93.063816

I. INTRODUCTION

Photon correlation measurement has played an important role in physical science. Since the second-order correlation (SOC) or two-photon correlation measurement was first devised by Hanbury-Brown and Twiss to resolve the size of stars [1], it has been utilized in various fields, from ultracold atomic systems [2] to single-molecule fluorescence [3]. As more efficient measurement schemes have been developed [4], many researchers has begun to address higher-order correlation functions in various aspects. M. Assmann *et al.* [5] observed higher-order photon bunching effects in a semiconductor microcavity laser. Asymmetric temporal behavior of three-photon correlation in a strongly driven atom-cavity system was studied by M. Koch *et al.* [6]. Higher-order photon correlation is also used in Doppler optical coherence tomography [7] as well as in high-order ghost imaging [8,9]. In matter-wave experiments, the third-order correlation of Bose-Einstein condensates was investigated to confirm its Bose statistics [10].

One of the main benefits obtainable from photon correlation measurement is information on the photon statistics. For instance, the normalized variance of photon statistics is simply described in terms of the SOC as $(\Delta n)^2/\langle n\rangle - 1 = \langle n\rangle(g^{(2)}(0)-1)$. Here, n is the photon number, $g^{(N)}(0)$ with $N=2$ is the second-order correlation, and the left-hand side is usually called the Mandel Q factor. The second-order and, furthermore, the higher-order correlation functions give us useful information on the photon statistics of a light source. In describing the statistical distribution of photon numbers, people frequently use the more generalized quantities called skewness and kurtosis, which are related to the third and fourth-order correlations, respectively. These quantities give graphical and intuitive information on the photon statistics, describing how much the distribution is asymmetrical and sharp, respectively.

In photon correlation measurements, N separate photodetectors are used for the Nth-order correlation function in most configurations. For SOC measurement, a Hanbury-Brown-Twiss-type measurement is often used. It might seem that this configuration would remove the detector dead-time effect because two successive photons detected at separate detectors appear to be free of the dead-time effect of each detector. Unfortunately, the dead-time effect on the SOC, nevertheless, exists even in this usual configuration and the distortion in the SOC is known to depend on the higher-order ($N \geqslant 3$) correlation functions [11–14]. From this consideration, one would expect that it might be possible to extract information on higher-order correlations from the SOC measurement by analyzing the dead-time effect. This possible new scheme to measure the correlation by using the detector dead-time effect is called "indirect measurement" throughout the paper.

However, most of the discussions in the literature [11–14] are restricted to the case where the light source is classical and the correlation time is much longer than the mean waiting time or the inverse of the photodetection flux. On the other hand, our previous study [15] considered the dead-time effect on nonclassical light but neglected the higher-order correlations in deriving a correction formula. It is thus desirable to generalize all of these previous studies to cover both nonclassical light sources and higher-order correlations.

In this paper, we theoretically derive an indirect measurement scheme for the third-order correlation by generalizing the previous studies on the dead-time effect. We then apply it to the three-photon correlation measurement in a cavity-QED (quantum electrodynamics) microlaser [16]. We observe a relation between $g^{(2)}(0)$ and $g^{(3)}(0,0)$ experimentally, which agrees well with our theoretical expectation.

This paper is organized as follows. In Sec. II, our indirect measurement scheme for the third-order correlation is theoretically discussed. We first show how the distortion of photodetection flux is connected to $g^{(2)}(0)$ and then extend the discussion to the distortion of $g^{(2)}(0)$ itself. This distortion eventually gives the information on the third-order correlation $g^{(3)}(0,0)$. In Sec. III, we then prove the relation $3(1-g^{(2)}(0)) \simeq 1 - g^{(3)}(0,0)$ in the cavity-QED microlaser when it operates at a large mean photon number. In the following section, we describe an experiment performed with the cavity-QED microlaser, where we extract $g^{(3)}(0,0)$ by using the indirect scheme and then show that the observed $g^{(3)}(0,0)$

*kwan@phya.snu.ac.kr

satisfies the above relation derived in Sec. III. Concluding remarks are given in Sec. IV.

II. THEORY OF THE INDIRECT MEASUREMENT SCHEME

In this section, we derive how the photodetection flux and $g^{(2)}(0)$ are distorted under the detector dead-time effect, which eventually provides a theoretical background for the indirect measurement scheme below.

A. $g^{(2)}(0)$ dependence of photodetection flux distortion

In this subsection, we first reveal that the dead-time effect on photodetection flux is related to $g^{(2)}(0)$, which is generalized to a relation between $g^{(3)}(0,0)$ and $g^{(2)}(0)$ in the subsequent subsection. Figure 1 depicts photodetection events in a two-detector configuration, where the black circles indicate observed photodetection events and the gray circles indicate missed events due to the detector dead time of duration τ. The second and fourth rows refer to the corresponding dead-time-free photodetection events. For further discussion, we hereby define

$$g'^{(N)}(t_{12},\ldots,t_{N-1,N};\phi_1,\ldots,\phi_N;\tau_1,\ldots,\tau_N), \tag{1}$$

an observed N-photon correlation function in the usual N-photodetector configuration when the dead-time-free photodetection flux and the dead time of the kth detector are denoted ϕ_k and τ_k, respectively. Here, $t_{k-1,k}$ means the photodetection time delay between the $(k-1)$th and the kth detector. For example, the correlation between the black circles in the first and third rows in Fig. 1 is given by $g'^{(2)}(t;\phi_{\rm st},\phi_{\rm sp};\tau_{\rm st},\tau_{\rm sp})$. When it comes to the correlation between the black circles in the first and those in the second rows (for the identical incident photon streams), it can be expressed as $g'^{(2)}(t;\phi_{\rm st},\phi_{\rm st};\tau_{\rm st},0)$.

The probability of finding dead-time-free photodetection events is apparently the sum of the probability of finding the black circles and the probability of finding the gray circles. The former is related to the observed photodetection flux $\phi'(\tau)$ with dead time τ. The conditional probability of finding a gray circle in a time interval t $(<\tau)$ after the appearance of a black circle is given by $g'^{(2)}(t;\phi,\phi;\tau,0)$. Note that the correlation between the black and the gray circles is the same as that between the observed events (black circles in the first and third rows) with associated flux $\phi'(\tau)$ and the corresponding dead-time-free events (black circles in the second and fourth rows) with associated flux ϕ. From this consideration, we derive the following relation:

$$\phi = \phi'(\tau) + \phi'(\tau)\phi\int_0^\tau g'^{(2)}(t;\phi,\phi;\tau,0)dt. \tag{2}$$

The first derivative of $\phi'(\tau)$ at $\tau = 0$ is then given by

$$\left.\frac{d\phi'(\tau)}{d\tau}\right|_{\tau=0} = -\phi^2 g'^{(2)}(0;\phi,\phi;0,0) = -\phi^2 g^{(2)}(0), \tag{3}$$

where we have used the relation

$$\frac{d}{d\tau}\int_0^\tau f(t,\tau)dt = f(\tau,\tau) + \int_0^\tau \frac{\partial f(t,\tau)}{\partial\tau}dt \tag{4}$$

in deriving Eq. (3), with $f(t,\tau)$ referring to an arbitrary multivariable function of t and τ. L. Mandel derived a formula similar to Eq. (2) for resonant fluorescence detection [17]. The only difference from our formula is that the integrand in Eq. (2) is $g^{(2)}(t)$, not $g'^{(2)}(t)$. This difference mainly comes from the fact that Mandel neglected the effect of the higher-order correlation.

B. $g^{(3)}(0,0)$ dependence of SOC distortion

In the following, we define the observed coincidence photodetection flux $\langle\phi'_{\rm st}(\tau_{\rm st})\phi'_{\rm sp}(\tau_{\rm sp})\rangle$, which refers to the number of simultaneous photodetection events at the start and stop detectors per unit time when the start and stop detectors have dead time $\tau_{\rm st}$ and $\tau_{\rm sp}$, respectively. Then $g'^{(2)}(0)$ measured in the two-detector configuration can be expressed as

$$g'^{(2)}(0;\phi_{\rm st},\phi_{\rm sp},\tau_{\rm st},\tau_{\rm sp}) = \frac{\langle\phi'_{\rm st}(\tau_{\rm st})\phi'_{\rm sp}(\tau_{\rm sp})\rangle}{\phi'_{\rm st}(\tau_{\rm st})\phi'_{\rm sp}(\tau_{\rm sp})}. \tag{5}$$

In Fig. 2, we illustrate how the coincidence photodetection flux is distorted by the dead time while assuming $\tau_{\rm st} = 0$ for simplicity. Missing of coincidence events occurs when events a and b (both are detected events) and event c (a missed event) satisfy the configuration depicted in Fig. 2(a). The probability of having three such events is apparently the same as the probability of having event a first and then events b and c

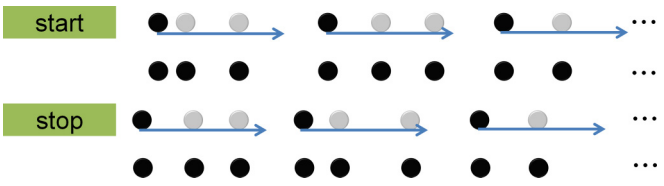

FIG. 1. Illustration of photodetection events and dead-time effect in a two-detector configuration. Black circles represent the observed photodetection events, whereas gray circles indicate the missed events caused by detector dead time, whose duration is shown by blue arrows. The correlation between the observed photodetection events (black circles in the first and third rows) corresponds to $g'^{(2)}(t)$. The second and fourth rows are copies of the first and third rows, respectively, without distinction between observed and missed photodetection events.

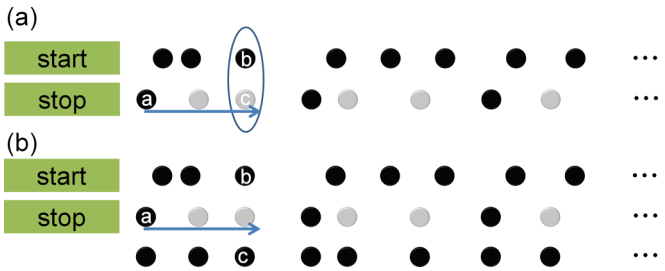

FIG. 2. (a) Illustration of the missed coincidence photodetection when only the stop detector has a dead time indicated by the blue arrow. For a photodetection scenario like a, b, and c, we miss a coincidence event. (b) A third row, a duplicate of the second row, has been added to show that the correlation among a, b, and c in (a) is the same as that in (b). Therefore, the correlation among these three events is given by $g'^{(3)}(t,0;\phi_{\rm sp},\phi_{\rm st},\phi_{\rm sp};\tau_{\rm sp},0,0)$.

simultaneously after time $t(<\tau_{sp})$ as depicted in Fig. 2(b), which is given by the expression

$$\phi_{st}\phi_{sp}\phi'_{sp}(\tau_{sp})g'^{(3)}(t,0;\phi_{sp},\phi_{st},\phi_{sp};\tau_{sp},0,0), \tag{6}$$

where $g'^{(3)}(t,0)$ approaches $g^{(3)}(t,0)$ as τ_{sp} decreases to 0. Accordingly, $\langle\phi'_{st}(0)\phi'_{sp}(\tau_{sp})\rangle$ and the dead-time-free coincidence photodetection flux $\langle\phi_{st}\phi_{sp}\rangle = \langle\phi'_{st}(0)\phi'_{sp}(0)\rangle$ satisfy the following relation

$$\langle\phi_{st}\phi_{sp}\rangle = \langle\phi'_{st}(0)\phi'_{sp}(\tau_{sp})\rangle + \phi_{st}\phi_{sp}\phi'_{sp}(\tau_{sp}) \times \int_0^{\tau_{sp}} g'^{(3)}(t,0;\phi_{sp},\phi_{st},\phi_{sp},\tau_{sp},0,0)dt. \tag{7}$$

Note that Eq. (7) still holds after exchanging the indices start and stop. Differentiating both sides by $\tau_{sp}(\tau_{st})$ at $\tau_{sp}(\tau_{st}) = 0$ then gives

$$\left.\frac{d\left\langle\phi'_{st}(0)\phi'_{sp}(\tau_{sp})\right\rangle}{d\tau_{sp}}\right|_{\tau_{sp}=0} = -\phi_{st}\phi_{sp}^2 g^{(3)}(0,0), \tag{8a}$$

$$\left.\frac{d\langle\phi'_{st}(\tau_{st})\phi'_{sp}(0)\rangle}{d\tau_{st}}\right|_{\tau_{st}=0} = -\phi_{sp}\phi_{st}^2 g^{(3)}(0,0), \tag{8b}$$

and thus, we can directly obtain the differentiation of Eq. (5), utilizing Eq. (3), as

$$\left.\frac{dg'^{(2)}(0;0,\tau_{sp})}{d\tau_{sp}}\right|_{\tau_{sp}=0} = \phi_{sp}([g^{(2)}(0)]^2 - g^{(3)}(0,0)), \tag{9a}$$

$$\left.\frac{dg'^{(2)}(0;\tau_{st},0)}{d\tau_{st}}\right|_{\tau_{st}=0} = \phi_{st}([g^{(2)}(0)]^2 - g^{(3)}(0,0)). \tag{9b}$$

In the linear approximation regime ($\phi\tau \ll 1$), we can express Eq. (5) as

$$g'^{(2)}(0;\tau_{st},\tau_{sp}) - g^{(2)}(0) \simeq \tau_{st}\left.\frac{\partial g'^{(2)}(0;\tau_{st},\tau_{sp})}{\partial\tau_{st}}\right|_{\tau_{st,sp}=0} + \tau_{sp}\left.\frac{\partial g'^{(2)}(0;\tau_{st},\tau_{sp})}{\partial\tau_{sp}}\right|_{\tau_{st,sp}=0}, \tag{10}$$

and thus

$$g'^{(2)}(0) - g^{(2)}(0) \simeq \{[g^{(2)}(0)]^2 - g^{(3)}(0,0)\}(\phi_{st}\tau_{st} + \phi_{sp}\tau_{sp}). \tag{11}$$

Combining Eq. (2) and Eq. (9) readily gives the second differentiation of $\phi'(\tau)$, and the result is

$$\left.\frac{d^2\phi'(\tau)}{d\tau^2}\right|_{\tau=0} = 2\phi^3 g^{(3)}(0,0) + \phi^2\left.\frac{dg^{(2)}(t)}{dt}\right|_{t=0}, \tag{12}$$

which clearly shows that the dead-time effect on photodetection flux also depends on the higher-order correlation. The first-order derivative of the SOC function at zero time delay, $\frac{dg^{(2)}(t)}{dt}|_{t=0}$, normally gives the inverse of the correlation time (an example is the cavity-QED microlaser), and thus Eq. (12) approaches Flammer and Ricka's result [14] in the limit of a long correlation time ($\tau_w \ll \tau_c$), where τ_w is the mean waiting time in consecutive photodetections.

Please note that $g'^{(2)}(0)$ is a function of $\phi_{st,sp}$ as well, but we omit these in the above equations for simplicity of expression. We do not give further consideration of $g'^{(2)}(0)$ with a large τ, for which the linear approximation no longer works. We should consider the fourth- or even higher-order correlations in this case, and that goes beyond the scope of the present work. We also neglect the dead-time effect on the temporal dependence of SOC, because in the linear approximation regime the correlation time is much longer than the dead time, and consequently the dead-time effect on the correlation time is negligible.

We have not assumed anything about the photon source until now. Therefore, all the results here can be applied to any kinds of photon sources. Particularly, Eq. (11), valid as long as $\phi\tau \ll 1$, is broadly applicable, as the information on $g^{(3)}(0,0)$ can be extracted from the first-order coefficient of $g'^{(2)}(0)$ as a function of the detector dead time.

The discussion heretofore can be generalized to the case of an N-detector configuration with only the Nth detector having the dead time τ_N. Then the following relation should hold:

$$\langle\phi_1\ldots\phi_N\rangle = \langle\phi'_1(0)\ldots\phi'_N(\tau_N)\rangle + \phi_1\ldots\phi_N\phi'_N(\tau_N) \times \int_0^{\tau_N} g'^{(N+1)}(0,\ldots,t,0;\phi_1,\ldots,\phi_{N-2},\phi_N, \times\phi_{N-1},\phi_N;0,\ldots,0,\tau_N,0,0)dt. \tag{13}$$

Differentiating both sides by τ_N gives

$$\left.\frac{dg'^{(N)}(0;0,\ldots,\tau_N)}{d\tau_N}\right|_{\tau_N=0} = \phi_N[g^{(2)}(0)g^{(N)}(0) - g^{(N+1)}(0)]. \tag{14}$$

The subscripts N can be replaced with arbitrary indices i ($1 \leqslant i \leqslant N$), and thus

$$\left.\frac{dg'^{(N)}(0;0,\ldots,\tau_i,\ldots,0)}{d\tau_i}\right|_{\tau_i=0} = \phi_i(g^{(2)}(0)g^{(N)}(0) - g^{(N+1)}(0)). \tag{15}$$

Finally, under the linear approximation $\phi_i\tau_i \ll 1$ we obtain

$$g'^{(N)}(0) - g^{(N)}(0) \simeq [g^{(2)}(0)g^{(N)}(0) - g^{(N+1)}(0)]\left(\sum_{i=1}^{N}\phi_i\tau_i\right). \tag{16}$$

This is a generalized form of Eq. (11). Note that we omit the detector dead times in the argument of the observed correlation function for simplicity.

According to Eq. (16), the constant term and the first-order coefficient of $g'^{(N)}(0)$ as a function of the dead times $\{\tau_i\}$ provide the information on the dead-time-free $g^{(N)}(0)$ and $g^{(N+1)}(0)$, respectively. The detector dead time is fixed in general. However, we can emulate various detector dead times on the record of observed photodetection events by deliberately deleting events. By plotting $g'^{(N)}(0)$ as a function of these emulated dead times, we can then extract both the dead-time-free $g^{(N)}(0)$ and the dead-time-free $g^{(N+1)}(0)$. The detailed procedure is presented in Sec. IV.

III. PHOTON CORRELATION IN THE CAVITY-QED MICROLASER

The cavity-QED microlaser is a microscopic laser consisting of a high-Q optical cavity and a beam of two-level atoms traversing the cavity mode. The two-level atoms pumped by a conventional laser serve as the gain medium. It is an optical analogy of the micromaser [18]. In the cavity-QED microlaser, lasing is possible even when only one atom on average [16] or a true single atom [19] is present in the cavity. The coherent interaction between atoms and the cavity mode is still maintained even when the mean atom number in the cavity is much larger than unity [20], exhibiting novel properties such as quantum jumps [21], sub-Poisson photon statistics [22], the atomic Šolc filter [23,24], and quantum frequency pulling [25,26] distinct from the conventional laser.

Quantum micromaser theory (QMT) [27] and semiclassical rate equation analysis predict various interesting features of the cavity-QED microlaser. The oscillatory gain function as the photon number of the cavity-QED microlaser represents the coherent interaction between the atom and the cavity mode, mainly accounting for the non-Poissonian properties of its intracavity photon statistics. The experiment done by W. Choi *et al.* [22] successfully observed these properties.

In this section, we show that $g^{(2)}(0)$ and $g^{(3)}(0,0)$ satisfy a simple relation when the cavity-QED microlaser is operating at a large mean photon number. Let us first note that $g^{(3)}(0,0)$ can be expressed as follows in general:

$$g^{(3)}(0,0) = \frac{\langle n^3\rangle - 3\langle n^2\rangle + 2\langle n\rangle}{\langle n\rangle^3}. \tag{17}$$

Meanwhile, the skewness γ of photon statistics is defined as

$$\gamma = \frac{\langle n^3\rangle - 3\langle n^2\rangle\langle n\rangle + 2\langle n\rangle^3}{\langle \Delta n\rangle^3}. \tag{18}$$

We can rewrite Eq. (17) in terms of the skewness as

$$g^{(3)}(0,0) = 1 + \frac{3Q}{\langle n\rangle} - \frac{(3Q+1)}{\langle n\rangle^2} + \frac{(Q+1)^{3/2}}{\langle n\rangle^{3/2}}\gamma. \tag{19}$$

In the following, we only consider the case where the Mandel Q factor is not close to 0 since the cavity-QED microlaser shows non-Poissonian photon statistics except for a few special atom numbers. In the case where $\langle n\rangle$ is much larger than $|Q|$ [i.e., $|1 - g^{(2)}(0)| \ll 1$], the third term in Eq. (19) becomes negligibly small compared to the second term. The skewness contained in the last term reflects the degree of asymmetry of the distribution. It becomes 0 for a perfectly symmetrical distribution whose median and mean are the same, such as a Gaussian or a delta-function distribution. With a large mean photon number and with a nearly symmetric photon number distribution, we can also neglect the last term in Eq. (19) compared with the second term.

The photon statistics of the micromaser as well as the cavity-QED microlaser have been calculated in many previous studies [28,29]. Under the condition that the atom number is large enough to generate a large intracavity mean photon number but still insufficient to lead to a quantum jump, all of the previous studies give a symmetric single-peak distribution, which implies that the skewness may have a tiny value. Based on QMT, we calculated the skewness for the cavity-QED microlaser in the case where $\langle n\rangle$ is sufficiently large (Fig. 3), where $\gamma_{\rm cqm}$ is the skewness (black dots) of the cavity-QED microlaser photon statistics at various atom numbers N_a, and $\gamma_{\rm poi} = \langle n\rangle^{-1/2}$ is that of the corresponding Poisson distribution (red dots) having the same mean photon number.

Figure 3 reveals that the order of magnitude of $\gamma_{\rm cqm}$ is similar to or less than that of $\gamma_{\rm poi}$ when $\langle n\rangle$ is large enough. Therefore, we can now neglect the last term in Eq. (19) for the cavity QED microlaser as well, as long as it operates well away from the regions where quantum jumps occur. Equation (19) is then approximated as

$$g^{(3)}(0,0) \simeq 1 + \frac{3Q}{\langle n\rangle} \tag{20}$$

for a large mean photon number. Equation (20) then readily gives

$$3(1 - g^{(2)}(0)) \simeq 1 - g^{(3)}(0,0) \tag{21}$$

because we have $g^{(2)}(0) = 1 + Q/\langle n\rangle$ by definition. The relation can also be expressed as

$$[g^{(2)}(0)]^3 \simeq g^{(3)}(0,0) \tag{22}$$

since we already assume that $g^{(2)}(0)$ and $g^{(3)}(0,0)$ are close to unity. Direct calculation of $g^{(2)}(0)$ and $g^{(3)}(0,0)$ based on QMT also gives a result consistent with ours [30].

Meanwhile, QMT completely ignores nonideal effects including the cavity dissipation and atomic velocity distributions. For this reason, the validity of Eq. (20) might be questioned under the realistic conditions since nonideal effects would considerably change the photon statistics. However, we expect that there is no dramatic change, at least in the symmetric shape of the photon number distribution, based on the following reasoning.

Incoherent and inhomogeneous effects tend to reduce the oscillatory behavior of the gain function. One example can be found in Ref. [31], where, with inclusion of the atomic velocity distribution, the amplitude of the gain function decreases as $\langle n\rangle$ increases. As these effects become severe, the gain function of the cavity-QED microlaser will approach that of the conventional laser whose photon statistics is Poissonian, and thus the skewness of the cavity-QED microlaser will get closer to $\gamma_{\rm poi}$. Therefore, we can still have $\gamma_{\rm cqm} \sim \langle n\rangle^{-1/2}$ and thus Eq. (20) under nonideal effects. To summarize, although nonideal effects evidently influence the photon statistics, Eq. (21) still holds.

By plugging Eq. (22) into Eq. (11) we then obtain

$$g'^{(2)}(0) - g^{(2)}(0) = \{[g^{(2)}(0)]^2 - [g^{(2)}(0)]^3\}(\phi_{\rm st} + \phi_{\rm sp})\tau, \tag{23}$$

where we assume $\tau = \tau_{\rm st} = \tau_{\rm sp}$. Since $g^{(2)}(0)$ is close to unity, Eq. (23) is numerically equivalent to

$$g'^{(2)}(0) \simeq g^{(2)}(0)\{1 + [1 - g^{(2)}(0)](\phi_{\rm st} + \phi_{\rm sp})\tau\}, \tag{24}$$

which is the result independently derived in Ref. [15].

The result obtained in this section is specific to the cavity-QED microlaser in the large-photon-number limit. Although the result is not general, it can still serve as a cross-check reference for the indirect measurement method discussed in

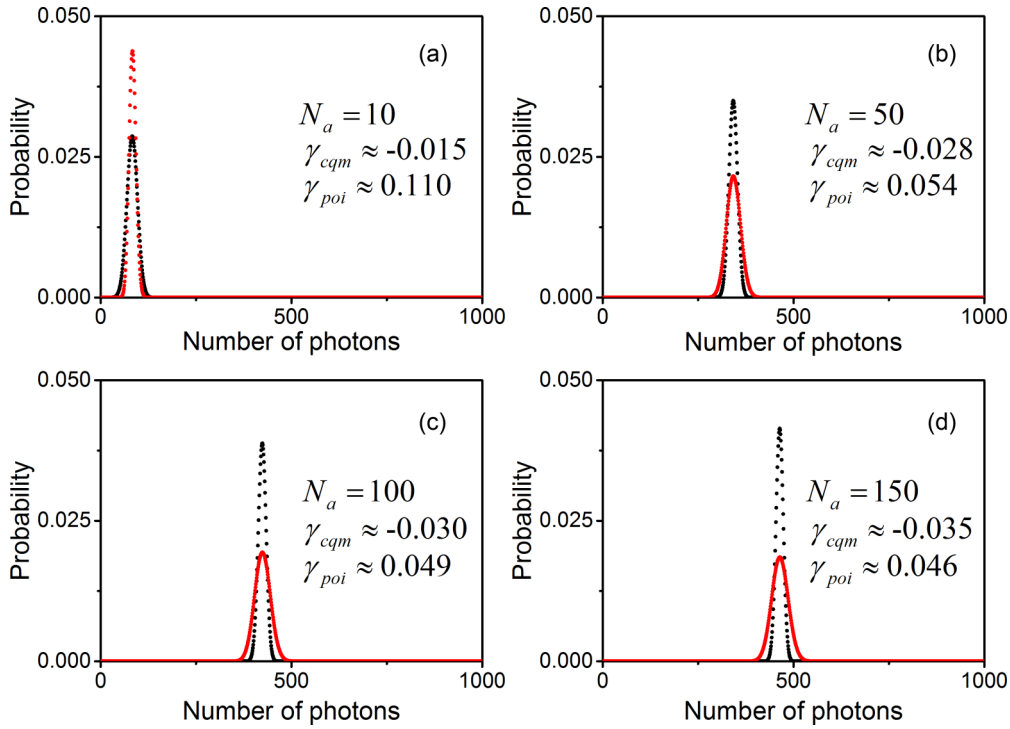

FIG. 3. Photon statistics of the cavity-QED microlaser operating in the large-photon-number region (black dots), well away from the regions where quantum jumps occur, compared to the Poissonian distributions (red dots) that have the same mean photon number. Here, N_a refers to the mean atom number. The photon statistics of the cavity-QED microlaser shows a near-symmetric single-peak distribution in both (a) super-Poissonian and (b–d) sub-Poissonian regions when the mean photon number is sufficiently large. Skewness values of the cavity-QED microlaser are similar to or less than the $\gamma_{\rm poi}$ of the Poissonian distributions. The coupling constant and interaction time between the cavity mode and the impinging atoms assumed in the calculation were $2\pi \times 190$ kHz and 0.1 μs, respectively, while the cavity line width was assumed to be 138 kHz. These operating parameters are basically the same as in Ref. [22].

the previous section and the experimental results discussed in the following sections.

IV. RESULTS AND DISCUSSION

A. $g^{(3)}(0,0)$ measurement of the cavity-QED microlaser

In typical photon-counting SOC measurements, the detector dead time is fixed for a given detector. Nonetheless, we can simulate various detector dead times by computationally deleting photodetection events in the observed photodetection records. Even with this approach, we still miss photodetection events near the origin within the physical detector dead time. However, if $g'^{(2)}(0)$ as a function of the dead time τ shows sufficiently linear variation near the origin, one can then approximate its variation in low-order polynomials of τ and obtain reliable values of the constant term and the first-order coefficient by performing a least-chi-square fitting.

Our experimental setup is basically the same as that in Ref. [15]. Figure 4(a) shows $g'^{(2)}(0)$ as a function of the dead time measured in the regime of sub-Poisson photon statistics of the cavity-QED microlaser. A similar plot appeared in our previous work [15]. The red square was obtained in the experiment where the mean photon number of the cavity-QED microlaser was approximately 600. Observed photodetection fluxes on the start and stop photodetectors are 2.6 Mcps (mega counts per second) and 3.3 Mcps, respectively, and the dead time is 28 ns for both detectors. The dead-time-free photodetection flux was calculated using Eq. (2) in Ref. [15] while approximately treating the output of the cavity-QED microlaser operating at a large mean photon number as coherent light. We simulated the prolonged dead times, corresponding to the black circles, in the same way as in Ref. [15]. The prolonged dead times imposed on both detectors were the same. At the photodetection fluxes given above, the emulated $g'^{(2)}(0)$ increases almost linearly until the 128-ns dead time. The fitting errors for the black circles are roughly 10% of $|1 - g'^{(2)}(0)|$.

In Fig. 4(b) we performed a least-chi-square fit of the data points in Fig. 4(a) with a second-order polynomial (a parabolic curve) from the red square to the 14th black circle, corresponding to the 128-ns dead time. Here, the x axis refers to the number of data points participating in the fit. Since the number of data points is limited in Fig. 4(a), fitting with polynomials higher than third order tends to give a fitting error larger than the fitting parameters. From the values of $g^{(3)}(0,0)$ and $g^{(2)}(0)$ in Fig. 4(b), we then obtain the ratio $[1 - g^{(3)}(0,0)]/[1 - g^{(2)}(0)]$ as shown in Fig. 4(c). We observed that the relation $3[1 - g^{(2)}(0)] \simeq 1 - g^{(3)}(0,0)$ in Eq. (21) is well satisfied with a reasonably large number of data points used in the fitting. The observed ratio with the fitting to the 14th data point was 2.98 ± 0.07. The error bars in Figs. 4(b) and 4(c) indicate the fitting errors.

We have also performed the $g^{(3)}(0,0)$ measurement with super-Poissonian light. Data in Fig. 5 correspond to $g'^{(2)}(0)$

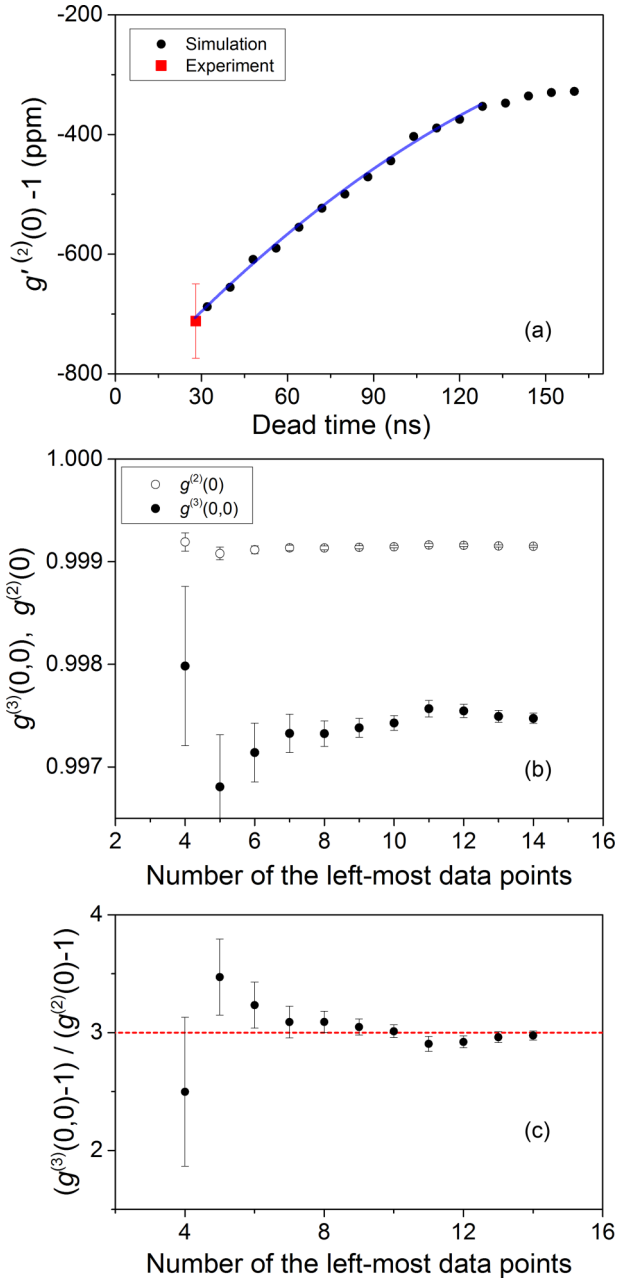

FIG. 4. (a) Relation between $g'^{(2)}(0)$ and dead time, observed by experiment and by prolonged dead times. Red squares indicate experimentally observed results in the cavity-QED microlaser. Observed photodetection fluxes at each detector were 2.6 and 3.3 Mcps, respectively. We simulated the prolonged dead-time results (black circles) by deleting photodetection events from the actual data. The resulting $g'^{(2)}(0)$ is almost linearly increasing up to 128 ns dead time. The solid blue line indicates the least-chi-square fit curve when the data points up to the 14th participate in the fitting process. (b) Values of $g^{(3)}(0,0)$ (filled circles) and $g^{(2)}(0)$ (open circles) obtained by performing second-order polynomial fitting over the data points in (a) and by using Eq. (11). Here, the horizontal coordinate indicates the number of data points participating in the fitting process. (c) Ratio of $g^{(3)}(0,0)-1$ to $g^{(2)}(0)-1$ based on the results in (b). The higher the number of data points used in the fitting, the more reliable the results will become. Eventually the ratio converges to the theoretical expectation (dashed red line). The mean photon number in the cavity was roughly 600.

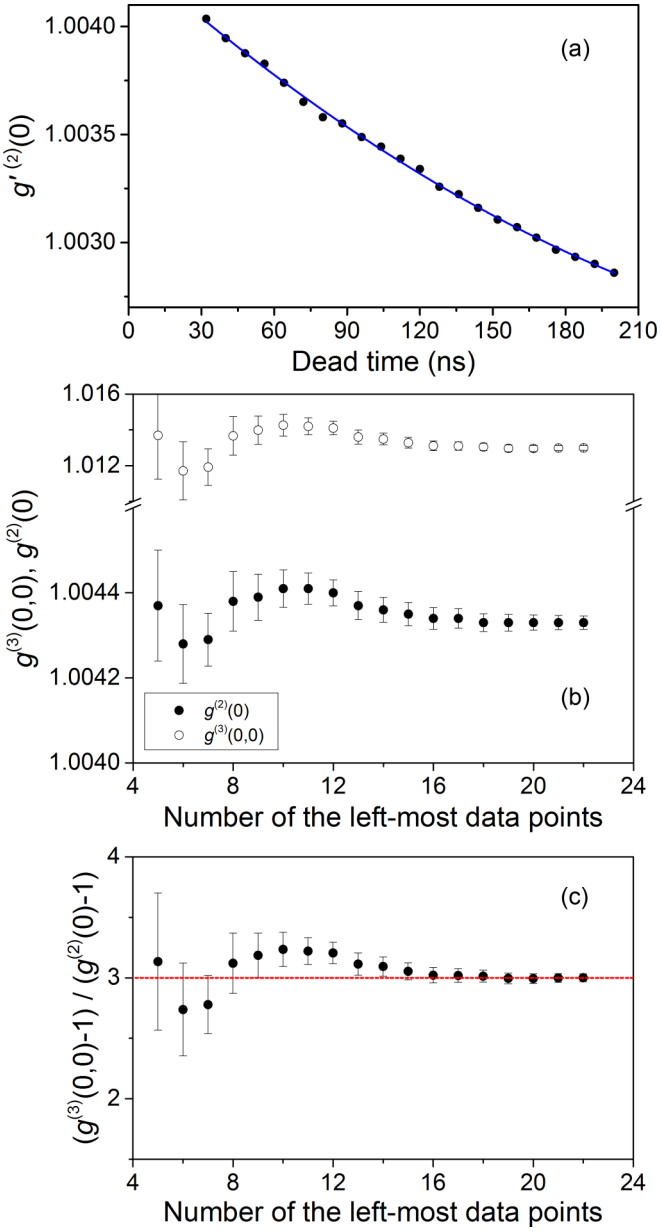

FIG. 5. (a) Relation between $g'^{(2)}(0)$ and the dead time, observed in the super-Poissonian regime of the cavity-QED microlaser (black circles). (b) Values of $g^{(3)}(0,0)$ (open circles) and $g^{(2)}(0)$ (filled circles) obtained by performing second-order polynomial fitting over the data points in (a) and by using Eq. (11). Fitting errors for individual black circles are less than 1% of $g'^{(2)}(0)-1$. Here, the horizontal coordinate indicates the number of data points participating in the fitting process. The solid blue line in (a) is the second-order polynomial fitting curve when all the presented data points are involved in the fitting process. (c) Ratio of $g^{(3)}(0,0)-1$ to $g^{(2)}(0)-1$. The obtained values of $|1-g^{(3)}(0,0)|/|1-g^{(2)}(0)|$ from the fitting with all data points is 3.00 ± 0.03.

measurements of the cavity-QED microlaser with a reduced mean intracavity atom number so as to generate super-Poissonian photon statistics. The observed photodetection fluxes were 870 kcps (kilo counts per second) and 1380 kcps for the start and stop detectors, respectively. The intracavity mean photon number for each data point was about 200. We

obtained $g^{(3)}(0,0)$ and $g^{(2)}(0)$ the same way as for Fig. 4. The fitting range was restricted up to the 200-ns dead time. The solid blue line is a second-order polynomial fit curve. The value of $|1 - g^{(3)}(0,0)|/|1 - g^{(2)}(0)|$ obtained in the fitting is 3.00 ± 0.03 when the data points up to 200 ns dead time are involved in the fitting, again well consistent with the theoretical expectation of Eq. (21). The dark count was only 500 cps and the contribution of the afterpulse was only 0.5% of the total photodetection flux, so we did not consider their effects in our data analysis.

B. Advantage of the current indirect measurement scheme

In the usual N-detector configuration for Nth-order correlation measurement, the signal-to-noise ratio (SNR) is given by $\sqrt{(T_0/\tau_w)^N/(T_0/t_b)^{N-1}} = \sqrt{(T_0/\tau_w)(t_b/\tau_w)^{N-1}}$ [15], where t_b is the bin time used in the calculation of the Nth-order correlation function and T_0 is the total measurement time. The bin time t_b should be small enough to resolve the temporal dependence of the correlation function, and thus it typically satisfies $t_b \ll \tau_w$. Therefore, in order to get a comparable SNR for the third-order correlation compared with the SOC measurement, the measurement time should be increased by a factor of τ_w/t_b. However, if the measurement time T_0 is limited for some technical reason such as a finite oven lifetime as in the cavity-QED microlaser, third-order correlation measurement will then be impossible. In this regard, our approach presented here provides a useful alternative for measurement of the higher-order ($N > 2$) correlation.

V. CONCLUSION

We have developed a universally applicable theory which describes how the dead time distorts the second-order photon correlation in the usual two-detector configuration. Our formula relates $g^{(2)}(0)$ and $g^{(3)}(0,0)$ to $g'^{(2)}(0)$ as a function of the dead time, and thus, we can measure unknown $g^{(3)}(0,0)$ from $g'^{(2)}(0)$. We call this new approach of obtaining $g^{(3)}(0,0)$ indirect measurement. In order to check the validity of our theory, we carried out an experiment with the cavity-QED microlaser in the large-photon-number regime and obtained $g^{(2)}(0)$ and $g^{(3)}(0,0)$ from $g'^{(2)}(0)$ utilizing our formula. Meanwhile, we have also shown that the cavity-QED microlaser satisfies $3(1 - g^{(2)}(0)) \simeq 1 - g^{(3)}(0,0)$ when it operates at a large intracavity photon number. The observed $g^{(2)}(0)$ and $g^{(3)}(0,0)$ values in our experiments agree well with the relation, thereby confirming the validity of our indirect measurement scheme. Since our indirect approach is based on second-order correlation measurement, it can greatly reduce the otherwise-much-longer measurement time for the third-order correlation for a desired SNR, and thus it is particularly useful when the operation time of the photon source is limited for some scientific or technical reason.

ACKNOWLEDGMENTS

This work was supported by a grant from Samsung Science and Technology Foundation under Project No. SSTF-BA1502-05.

[1] E. Hanbury Brown and R. Q. Twiss, Correlation between photons in two coherent beams of light, Nature (London) **177**, 27 (1956).

[2] S. Fölling, F. Gerbier, A. Widera, O. Mandel, T. Gericke, and I. Bloch, Spatial quantum noise interferometry in expanding ultracold atom clouds, Nature **434**, 481 (2005).

[3] R. Ververk and M. Orrit, Photon statistics in the fluorescence of single molecules and nanocrystals: Correlation functions versus distributions of on- and off-times, J. Chem. Phys. **119**, 2214 (2003).

[4] W. Choi, M. Lee, Y.-R. Lee, C. Park, J.-H. Lee, and K. An, Calibration of second-order correlation functions for non-stationary sources with a multi-start multi-stop time-to-digital converter, Rev. Sci. Instrum. **76**, 083109 (2005).

[5] M. Assmann, F. Veit, M. Bayer, M. Poel, and J. M. Hvam, Higher-order photon bunching in a semiconductor microcavity, Science **325**, 297 (2009).

[6] M. Koch, C. Sames, M. Balbach, H. Chibani, A. Kubanek, K. Murr, T. Wilk, and G. Rempe, Three-Photon Correlations in a Strongly Driven Atom-Cavity System, Phys. Rev. Lett. **107**, 023601 (2011).

[7] L. Huang, Z. Ding, W. Hong, C. Wang, and T. Wu, Higher-order cross-correlation-based Doppler optical coherence tomography, Opt. Lett. **36**, 4314 (2011).

[8] K. W. C. Chan, M. N. O'Sullivan, and R. W. Boyd, High-order thermal ghost imaging, Opt. Lett. **34**, 3343 (2009).

[9] K. W. C. Chan, M. N. O'Sullivan, and R. W. Boyd, Optimization of thermal ghost imaging: high-order correlations vs. background subtraction, Opt. Exp. **18**, 5562 (2010).

[10] S. S. Hodgman, R. G. Dall, A. G. Manning, K. G. H. Baldwin, and A. G. Truscott, Direct measurement of long-range third-order coherence in Bose-Einstein condensates, Science **331**, 1046 (2011).

[11] K. Schatzel, Dead time correction of photon correlation functions, Appl. Phys. B **41**, 95 (1986).

[12] K. Schatzel, R. Kalstrom, B. Stampa, and J. Ahrens, Correction of detection-system dead-time effects on photon-correlation functions, J. Opt. Soc. Am. B **6**, 937 (1989).

[13] E. Overbeck, C. Sinn, I. Flammer, and J. Ricka, Silicon avalanche photodiodes as detectors for photon correlation experiment, Rev. Sci. Instrum. **69**, 3515 (1998).

[14] I. Flammer and J. Ricka, Dynamic light scattering with single-mode receivers: Partial heterodyning regime, Appl. Opt. **36**, 7508 (1997).

[15] B. M. Ann, Y. Song, J. Kim, D. Yang, and K. An, Correction for the detector-dead-time effect on the second-order correlation of stationary sub-Poissonian light in a two-detector configuration, Phys. Rev. A **92**, 023830 (2015).

[16] K. An, J. J. Childs, R. R. Dasari, and M. S. Feld, Microlaser: A Laser with one Atom in an Optical Resonator, Phys. Rev. Lett. **73**, 3375 (1994).

[17] R. Short and L. Mandel, Observation of Sub-Poissonian Photon Statistics, Phys. Rev. Lett. **51**, 384 (1983).
[18] D. Meschede, H. Walther, and G. Müller, One-Atom Maser, Phys. Rev. Lett. **54**, 551 (1985).
[19] M. Lee, J. Kim, W. Seo, H.-G. Hong, Y. Song, R. R. Dasari, and K. An, Three-dimensional imaging of cavity vacuum with single atoms localized by a nanohole array, Nat. Commun. **5**, 3441 (2014).
[20] K. An, Validity of single-atom approximation in the many-atom microlaser, J. Phys. Soc. Jpn. **72**, 811 (2003).
[21] C. Fang-Yen, C. C. Yu, S. Ha, W. Choi, K. An, R. R. Dasari, and M. S. Feld, Observation of multiple thresholds in the many-atom cavity QED microlaser, Phys. Rev. A **73**, 041802(R) (2006).
[22] W. Choi, J.-H. Lee, K. An, C. Fang-Yen, R. R. Dasari, and M. S. Feld, Observation of Sub-Poisson Photon Statistics in the cavity-QED Microlaser, Phys. Rev. Lett. **96**, 093603 (2006).
[23] H.-G. Hong, W. Seo, M. Lee, Y. Song, Y.-T. Chough, J.-H. Lee, and K. An, Atomic Šolc filter: Multi-resonant photoemission via periodic poling of atom-cavity constant, Opt. Express **17**, 15455 (2009).
[24] W. Seo, H.-G. Hong, M. Lee, Y. Song, Y.-T. Chough, W. Choi, C. Fang-Yen, R. R. Dasari, M. S. Feld, J.-H. Lee, and K. An, Realization of a bipolar atomic Šolc filter in the cavity-QED microlaser, Phys. Rev. A **81**, 053824 (2010).
[25] H.-G. Hong and K. An, Quantum theory of frequency pulling in the cavity-QED microlaser, Phys. Rev. A **85**, 023836 (2012)
[26] H.-G. Hong, W. Seo, Y. Song, M. Lee, H. Jeong, Y. Shin, W. Choi, R. R. Dasari, and K. An, Spectrum of the Cavity-QED Microlaser: Strong Coupling Effects in the Frequency Pulling at off Resonance, Phys. Rev. Lett. **109**, 243601 (2012).
[27] P. Filipowicz, J. Javanainen, and P. Meystre, Theory of a microscopic maser, Phys. Rev. A **34**, 3077 (1986).
[28] L. Davidovich, Sub-Poissonian processes in quantum optics, Rev. Mod. Phys. **68**, 127 (1996).
[29] M. O. Scully and M. S. Zubairy, *Quantum Optics* (Cambridge University Press, Cambridge, UK, 1997).
[30] H.-G. Hong, Spectral Lineshape Measurement of the Cavity-QED Microlaser, Ph.D. thesis, Seoul National University, 2011.
[31] W. Choi, Nonclassical Photon Statistics in the Many-Atom Microlaser, Ph.D. thesis, Seoul National University, 2004.